Article

Redox-Responsive Biomimetic Polymeric Micelle for Simultaneous Anticancer Drug Delivery and Aggregation Induced Emission (AIE) Active Imaging

Jun Hu, Weihua Zhuang, Boxuan Ma, Xin Su, Tao Yu, Gaocan Li, Yanfei Hu, and Yunbing Wang

Bioconjugate Chem., **Just Accepted Manuscript** • DOI: 10.1021/acs.bioconjchem.8b00119 • Publication Date (Web): 02 May 2018

Redox-responsive Biomimetic Polymeric Micelle for Simultaneous Anticancer Drug Delivery and Aggregation Induced Emission (AIE) Active imaging

Jun Hu[1], Weihua Zhuang[1], Boxuan Ma, Xin Su, Tao Yu, Gaocan Li, Yanfei Hu*, Yunbing Wang*

National Engineering Research Center for Biomaterials, Sichuan University, 29 Wangjiang Road, Chengdu 610064, China

[1]These authors (Jun Hu and Weihua Zhuang) contributed equally to the work

E-mail: huyanfei@scu.cn and E-mail: yunbing.wang@scu.edu.cn.

ABSTRACT

Intelligent polymeric micelles have been developed as potential nanoplatforms for efficient drug delivery and diagnosis. Herein, we successfully prepared redox-sensitive polymeric micelles combined aggregation induced emission (AIE) imaging as an outstanding anticancer drug carrier system for simultaneous chemotherapy and bioimaging. The amphiphilic copolymer TPE-SS-PLAsp-*b*-PMPC could self-assemble into spherical micelles and these biomimetic micelles exhibited great biocompatibility and remarkable ability in anti-protein adsorption, showing great potential for biomedical application. Anticancer drug doxorubicin (DOX) could be encapsulated during the self-assemble process, and these drug-loaded micelles showed intelligent drug release and improved antitumor efficacy due to the quick disassembly in response to high level of glutathione (GSH) environment. Moreover, the intracellular DOX release could be traced through the fluorescent imaging of these AIE micelles. As expected, the *in vivo* antitumor study exhibited that these DOX-carried micelles showed better antitumor efficacy and less adverse effects than that of free DOX. These results strongly indicated that this smart biomimetic micelle system to be a prominent candidate for chemotherapy and bioimaging.

INTRODUCTION

Nanoparticles have been extensively employed as efficient drug carriers for cancer therapy with notable reduced side effects and improved therapeutic efficacy[1-3]. Well-designed polymeric nanoparticles with a size of 10-200 nm can spontaneously

accumulate in tumor tissue during the long-circulation *in vivo* due to the enhanced permeability and retention (EPR) effect[4-6], which has greatly facilitated the development of nanomedicine. Polymeric micelles, self-assembling from amphiphilic block copolymers, have been successfully used for the delivery of water-insoluble antitumor drugs, and several polymeric micelles have been reached to clinical trials[7-9]. However, the distribution of micelles *in vivo* is difficult to trace and the lack of intelligent drug release would reduce the therapeutic efficacy of antitumor drugs.

As a desired polymeric micelle, it should not only deliver antitumor drugs to the targeted site, but also trace the distribution of drug carriers *in vivo*. However, conventional micelles are usually invisible, which makes it difficult to monitor the track of drug carriers. Therefore, development of nanocarrier with high-efficiency fluorescence is urgent needed for drug delivery systems[10]. However, when traditional fluorescence agents are encapsulated into the core of nanoparticles, the well-known phenomenon, aggregation caused quenching (ACQ), leads to the reduction of fluorescence due to the "π-π stacking" of the rigid planar structures, which limit their further application in biomedical[11]. In 2001, Tang′s group first reported the aggregation-induced emission (AIE) effect of a new class of fluorescent molecule instead exhibiting strong luminescence in aggregated state [12]. This special property is widely utilized to overcome the defect of ACQ effect and make nanocarriers available for simultaneous cancer diagnostic and therapy[13-14].

Ideally, drug-loaded micelles are expected to rapid release the cargos to ensure efficient therapy effect after they accumulate in tumor sites. Therefore, intelligent

micelles with stimuli-sensitive features (e.g., redox, temperature, pH, and specific enzyme response)[15-18] are developed for target site-triggered drugs release in responding to the specific intracellular and extracellular environment of tumor tissues [19-22]. Disulfide-based redox responsiveness is widely used owing to the obvious difference in GSH concentration between the reducing intracellular space (approximately 2-10 mM) and mildly oxidizing in extracellular space (approximately 2-20 μM) of tumor cells[23-24]. Disulfide linkage will be quickly cleaved at high concentration of GSH in the intracellular environment of tumor cells, while keeping stable at a low concentration of GSH in the extracellular environment[25]. Taking advantage of this characteristic, disulfide linkage contained polymeric micelles have been developed for controlled delivery and intelligent release of anticancer drugs, resulting in enhanced antitumor efficacy[26].

The biocompatibility and stability during blood circulation of polymeric micelles are significant to drug delivery systems for increasing the accumulation of drugs[27]. In this context, functional and biological compatible shell of the polymeric micelles will prevent micelles from interaction with cells and proteins in the blood and avoid rapid renal clearance by reticuloendothelial system (RES)[28-29]. Numerous hydrophilic polymers with great biocompatibility are selected as shell-forming segments[30]. Among these polymers, hydrophilic poly (ethylene glycol) (PEG) is widely used as the hydrophilic shell due to its ability to form tight association with water molecules via hydrogen bond, giving "stealth" properties to micelles by generating a hydrating layer[31-32]. Apart from conventional PEG, zwitterionic phosphorylcholine based

polymers are often used for engineering the hydrophilic shell of micelles for their excellent biocompatibility, high hydrophily, superior biomimetic properties and splendid resistance to protein adsorption[33-34]. Phosphorylcholine based polymers, for instance, poly (2-methacryloyloxyethyl phosphorylcholine) (PMPC) has been successful introduced to several nanocarriers as shell-building blocks for drug delivery[35-37]. Due to its cell membrane-mimetic structure, PMPC is supposed to enhance cellular uptake of drug-loaded micelles[38].

In this work, we reported redox-sensitive polymeric micelles with AIE property for intelligent drug delivery and activated bioimaging (Scheme 1). Disulfide linkage contained TPE-conjugated poly (aspartic acid)-block-poly (2-methacryloyloxyethyl phosphorylcholine) (TPE-SS-PLAsp-*b*-PMPC) has been successful synthesized. TPE-SS-PLAsp-*b*-PMPC could self-assemble into core-shell structure with a diameter of 87.3 nm with fairly narrow size distribution. DOX is encapsulated into the core of micelles via hydrophobic interaction and π-π stacking with benzene rings of TPE during the self-assembly of the copolymer. The TPE groups inside the core of micelles endowed these micelles unique AIE property, which could be used for bioimaging. Furthermore, the stability, drug release behavior, cellular uptake, *in vitro* cytotoxicity and *in vivo* antitumor efficacy of these DOX-loaded TPE-SS-PLAsp-*b*-PMPC micelles were systematically studied and the results were relatively attractive and inspiring.

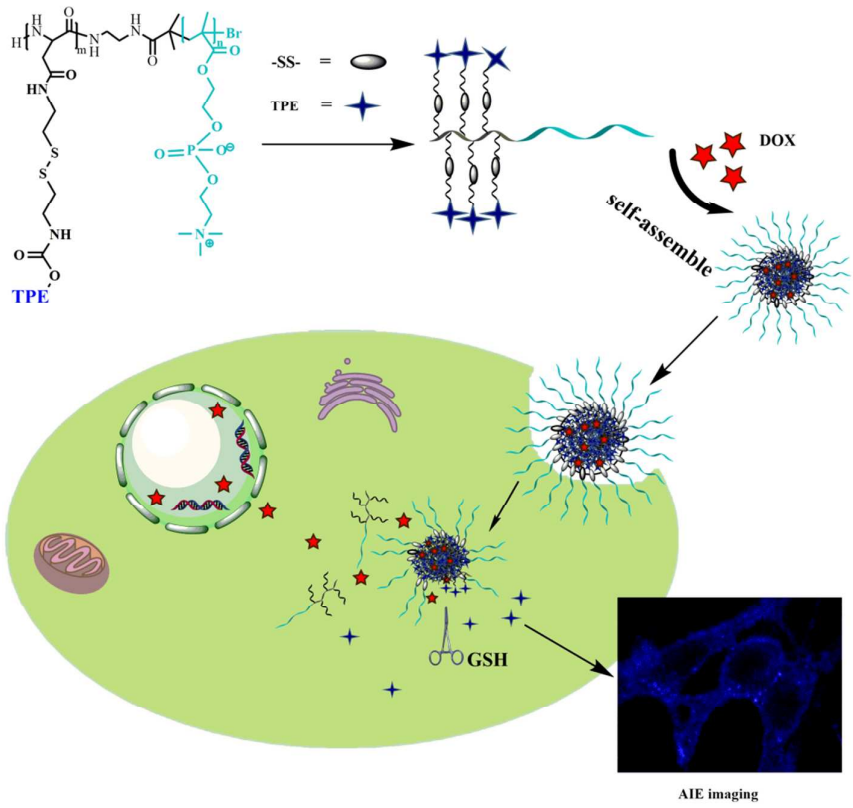

Scheme 1. Illustration of DOX-loaded TPE-SS-PLAsp-*b*-PMPC micelles, GSH-triggered drug release and AIE cell imaging.

RESULTS AND DISCUSSIONS

Synthesis of TPE-SS-PLAsp-*b*-PMPC

The ^{13}C NMR spectra of TPE-NO_2 was recorded in the Figure S1 and the high resolution mass spectrum (HR-MS) was further adopted for the structural confirmation of TPE- NO_2. The detailed synthetic route of TPE-SS-PLAsp-*b*-PMPC was shown in Scheme 2. First, ring opening polymerization (ROP) of BLA-NCA was performed using N-(2-aminoethyl)-2-bromo-2-methylpropanamide as functional initiator to obtain PBLAsp-Br macroinitiator. The ^{1}H NMR spectrum of PBLAsp-Br (Figure S2) proved the successful synthesis of PBLAsp-Br. The degree of

polymerization (DP) of PBLAsp-Br block was 18 as calculated from the integral ratio of the peaks at δ 1.80 ppm of methyl and δ 4.62 ppm of methyne. The molecular weight of the PBLAsp-Br was 4700 with a polymer dispersity index (PDI) of 1.39 measured by GPC using DMF as eluent (Figure S3). Second, PBLAsp-*b*-PMPC was obtained by ATRP of MPC using PBLAsp-Br as macroinitiator. The ^{1}H NMR spectrum result of PBLAsp-*b*-PMPC copolymer was showed in Figure S4, peaks at 7.32 ppm were assigned to benzene groups of PBLAsp block, the characteristic peaks at δ 3.3 ppm and peaks from 3.6-4.3 ppm were assigned to methyl and methylene groups of PMPC block. The DP of PMPC block was calculated to be 57 based on the integral ratio of the peaks at δ3.70 ppm of methylene group of PMPC block to that at δ7.32 ppm of benzene group from PBLAsp block. Third, benzyl groups of PBLAsp-*b*-PMPC were replaced by cystamines, and the total disappear of peaks of benzyl groups and methylenes (δ 5.12 ppm) in ^{1}H NMR spectrum of NH_2-SS-PLAsp-*b*-PMPC (Figure S5) demonstrated the successful synthesis of NH_2-SS-PLAsp-*b*-PMPC. Finally, TPE was conjugated to NH_2-SS-PLAsp-*b*-PMPC to obtain TPE-SS-PLAsp-*b*-PMPC. The ^{1}H NMR spectrum of TPE-SS-PLAsp-*b*-PMPC was shown in Figure 1, peaks of TPE were found at δ 6.90-7.50 ppm, and the characteristic peaks of PMPC were unabridged comparing to PBLAsp-*b*-PMPC, indicating the successful synthesis of TPE-SS-PLAsp-*b*-PMPC. The grafting degree of TPE was 16 as calculated from the integration ratio of peaks at δ 6.90-7.50 ppm of TPE to peaks at δ 3.71 ppm of PMPC blocks. Therefore, the copolymer named TPE_{16}-SS-$PLAsp_{18}$-*b*-$PMPC_{57}$ has been synthesized with the

molecular weight of 26200 g/mol.

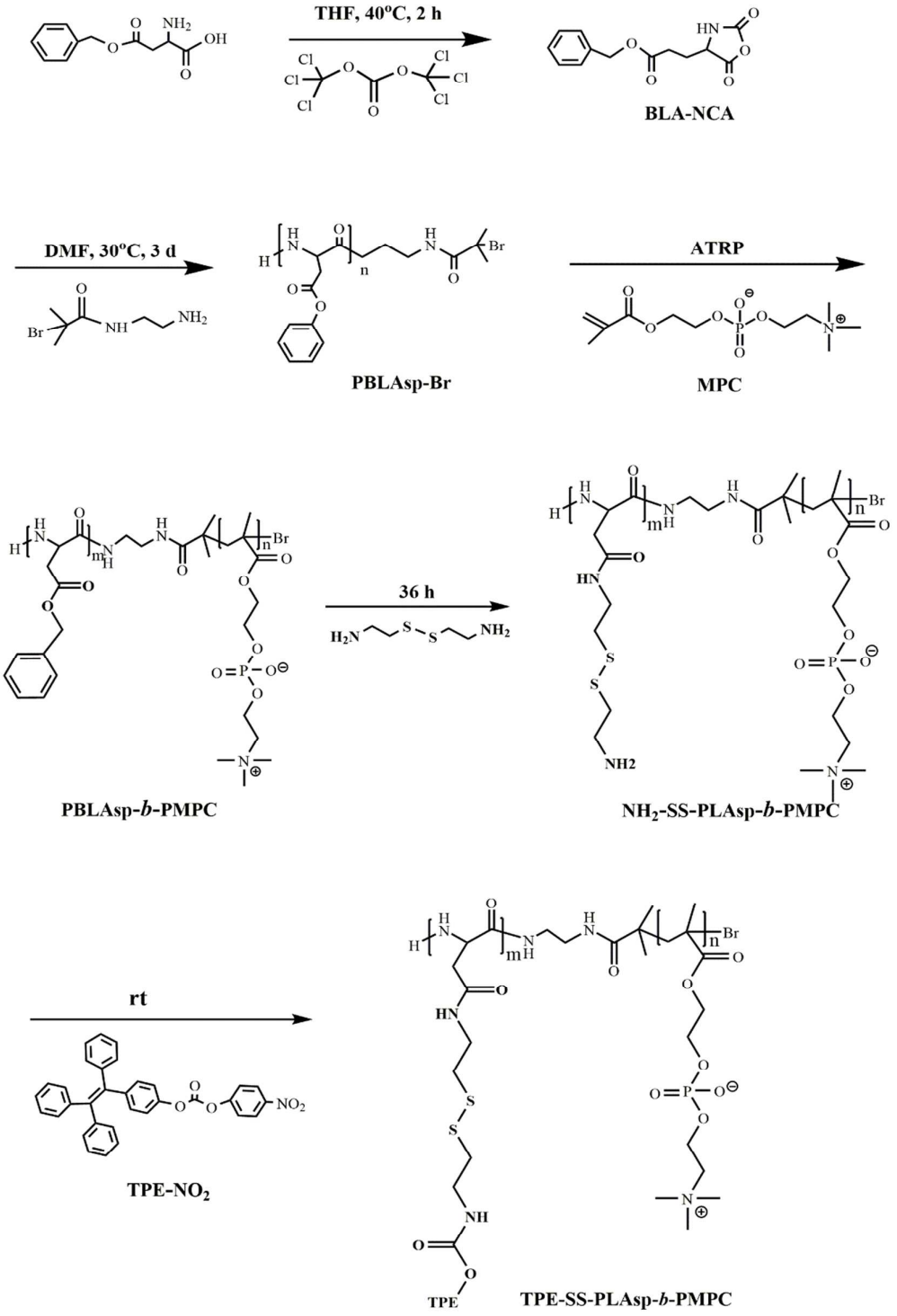

Scheme 2. Synthetic route of TPE-SS-PLAsp-*b*-PMPC.

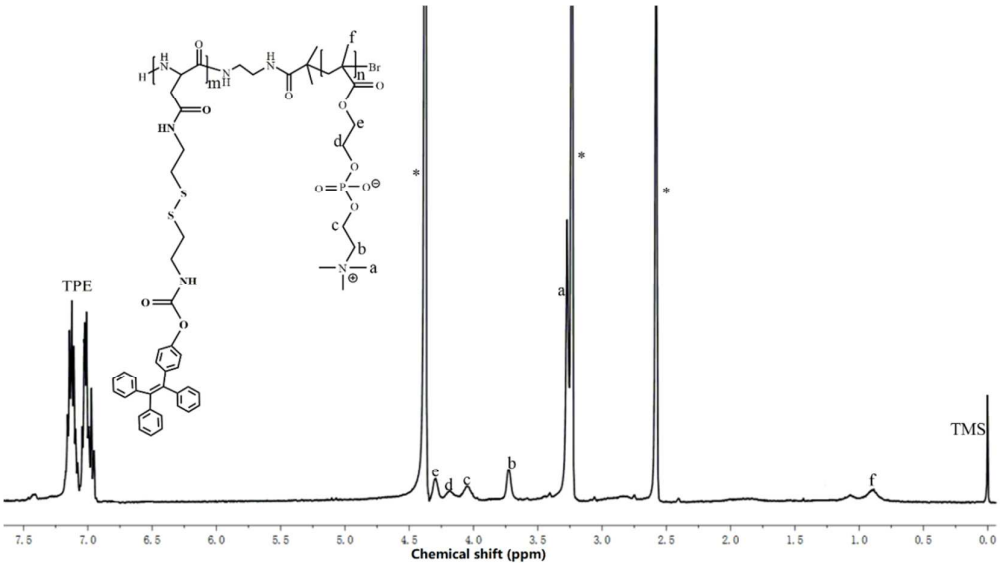

Figure 1. ^{1}H NMR spectrum of TPE-SS-PLAsp-*b*-PMPC in CD_3OD and DMSO-d_6 (1:1, V/V).

Preparation and Characterization of TPE-SS-PLAsp-*b*-PMPC Micelles

The amphiphilic copolymer TPE-SS-PLAsp-*b*-PMPC could self-assemble into core-shell micelles, which could be confirmed by the ^{1}H NMR result in D_2O. As shown in Figure S6, the peaks of TPE-SS-PLAsp blocks were totally disappeared, while the peaks of PMPC blocks could be observed. Besides, UV absorption spectra of TPE-SS-PLAsp-*b*-PMPC in different solvents were further applied to support the formulation of nanoparticles, level-off tails could be observed in the UV-Vis spectrum of TPE-SS-PLAsp-*b*-PMPC in H_2O in Figure S7, which were commonly observed in nanoparticle suspensions and due to the light scattering effect of the aggregates[36,45]. DOX was encapsulated into the core of TPE-SS-PLAsp-*b*-PMPC micelles due to the hydrophobic interaction and π-π stacking between DOX and TPE. As shown in Figure 2A, the particle size of TPE-SS-PLAsp-*b*-PMPC blank micelles was 87.3 nm with a PDI of 0.146 and the size of DOX-loaded micelles was 123.1 nm with a PDI of 0.135.

The increase of size indicated the successful encapsulation of DOX in micelles. The uniform spherical morphology of micelles was further observed by TEM (Figure 2E). The particle size of micelles in TEM image was smaller than that of DLS, which was due to the dehydration of the polymeric micelles during sample preparation for TEM. The DLC and DLE of TPE-SS-PLAsp-*b*-PMPC micelles were 5.6 % and 29.6 % as determined by UV spectroscopy, respectively.

Preparetion and Characterization of TPE-SS-PLAsp-b-PMPC Polymeric Micelles

To investigate the *in vitro* stability of polymeric micelles, blank micelles and DOX-loaded micelles were incubated in PBS with continuous oscillation for 48 h, and DOX-loaded micelles with 10% and 50% FBS (volume fraction) added were also studied under the same condition. As shown in Figure 2B, both blank micelles and DOX-loaded micelles exhibited excellent stability after incubation for 48 h and these DOX-loaded micelles also showed excellent anti-protein adhesion due to the biomimetic hydrophilic PMPC shell. The results in Figure 2B also demonstrated that these micelles would be stable during long circulation *in vivo*.

The micellar structure was supposed to be disintegrated in a medium contained high concentration of GSH due to the cleavage of disulfide bonds. DOX-loaded micelles were incubated with 10 mM GSH and DLS was employed to monitor the size changes of micelles. As shown in Figure 2C and Figure 2D, the DLS results of TPE-SS-PLAsp-*b*-PMPC micelles changed from unimodal peak to multimodal peaks with the obviously increased particle size, which indicated the destruction of micellar

structure and the formation of aggregates. The redox-response behavior of these micelles was further investigated by TEM. As shown in Figure 2F, obvious heterogeneous spherical micelles were observed after incubation in 10 mM GSH for 8 h, which was in accord with Figure 2C and Figure 2D.

AIE behavior of TPE-NO_2 was studied by fluorescence spectra in the mixture of THF and water with different water fraction. As shown in Figure 3A, the fluorescence intensity (FL) of TPE-NO_2 was gradually enhanced along with the increase of water fraction, suggesting the formulation the aggregates of TPE-NO_2, which restricted the free motions of TPE-NO_2 and exhibited strong fluorescence. AIE active fluorescent emission of micelles was investigated subsequently. TPE was restricted in the hydrophobic core during the formulation of micelles, and as expected, those micelles exhibited excellent fluorescent property in aqueous solutions, which would be suitable for bioimaging. As shown in Figure 3B, TPE-SS-PLAsp-*b*-PMPC micelles exhibited strong fluorescence in water, while the FL intensity would significantly reduce when the copolymers were dissolved in DMF solution (the water fraction decreased), owing to the disassembly of micelles, which set TPE groups free and the AIE effect was reduced. Moreover, FL spectra of DOX-loaded TPE-SS-PLAsp-*b*-PMPC micelle were also studied. As shown in Figure 3C, the FL intensity of both TPE and DOX were decreased compared to that of the same concentration of blank TPE-SS-PLAsp-*b*-PMPC micelle and free DOX, respectively. Moreover, with the increase of loaded DOX, the FL intensity of TPE was decreased with slightly emission peak blue shifting (Figure 3D), demonstrating the fluorescence resonance

energy transfer (FRET) effect between TPE and encapsulated drug DOX might be existed[46].

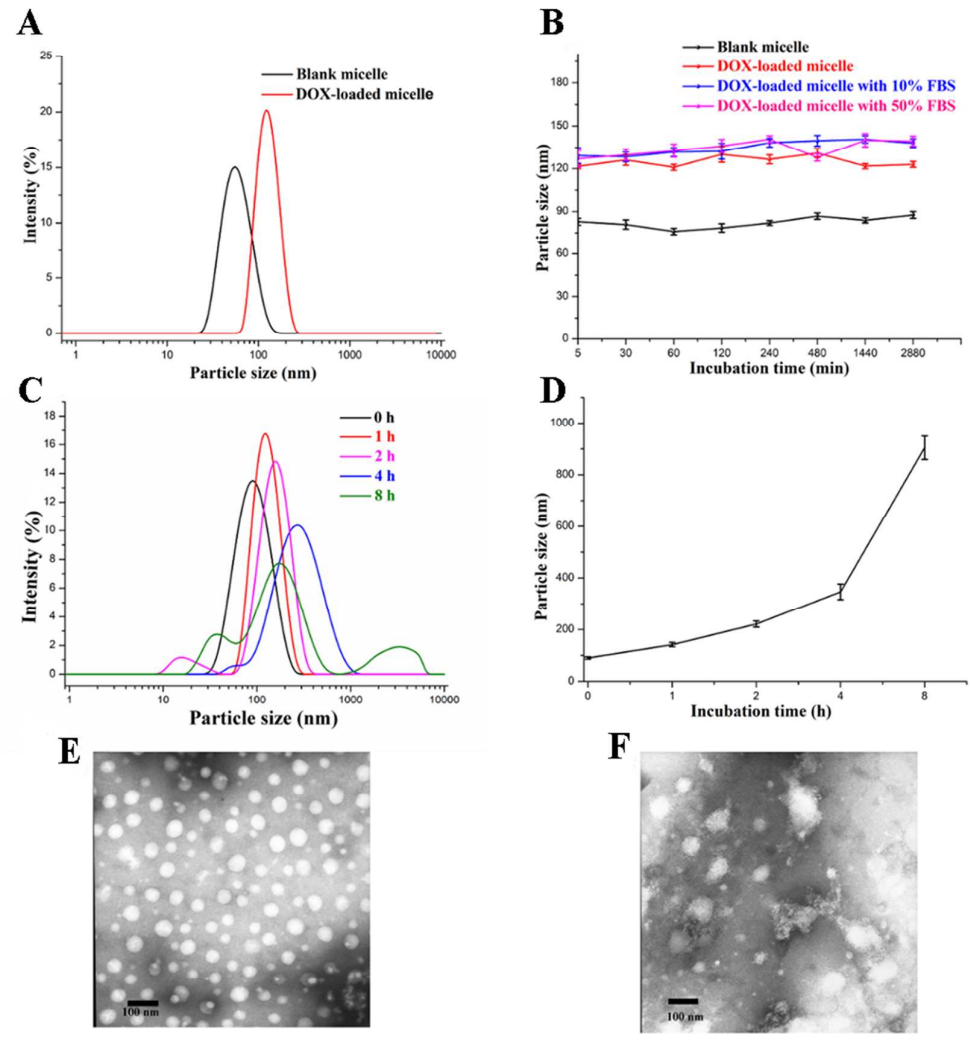

Figure 2. The particle size of blank micelle and DOX-loaded micelles (A). Particle size changes of micelles after different incubation time in different solution (B). Changes of size distribution and variation of TPE-SS-PLAsp-*b*-PMPC micelles incubated with 10 mM GSH (C) and (D). TEM image of DOX-loaded micelles (E). TEM image of DOX-loaded micelles treated with 10 mM GSH for 8 h (F).

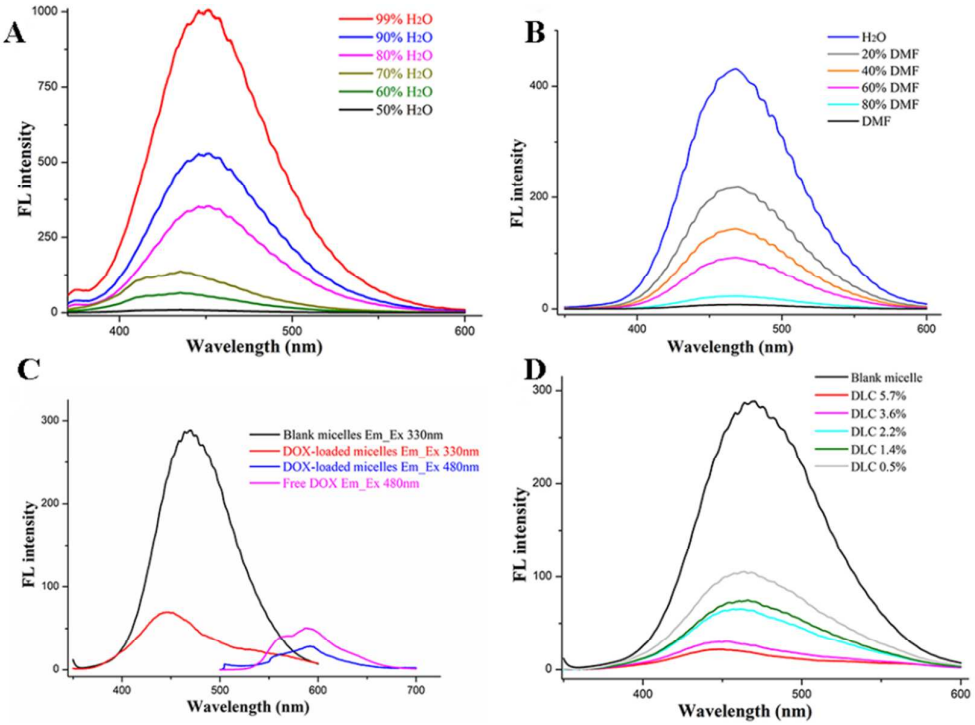

Figure 3. **A**) FL intensity of TPE- NO_2 in mixture of THF/water with different fraction of water (40 μM TPE-NO_2, λ_{ex} = 330 nm). **B**) FL intensity of TPE-SS-PLAsp-*b*-PMPC (40 μM TPE) in mixture of DMF/water with different fraction of water. **C**) FL spectra of TPE-SS-PLAsp-*b*-PMPC micelles (40 μM TPE), DOX-loaded TPE-SS-PLAsp-*b*-PMPC micelles (40 μM TPE, 2 μM DOX) and free DOX (2 μM). **D**) Fluorescence of DOX-loaded TPE-SS-PLAsp-*b*-PMPC micelles with different DOX loading content (λ_{ex} = 330 nm).

***In Vitro* Drug Release**

Antitumor drug was supposed to rapidly release as soon as drug-loaded nanocarriers reached tumor tissue. The GSH triggered drug release of DOX-loaded TPE-SS-PLAsp-*b*-PMPC micelles was performed in PBS buff saline solution with 10 mM GSH or without GSH. As shown in Figure 4, approximately 30% of drug was released in the medium without GSH after 48 h. On the contrary, more than 90 % of

DOX was released in 48 h. Thus, the release of DOX was much quicker in medium contained 10 mM GSH with more than 90% of DOX was released in 48 h, which would enhance antitumor efficacy. In addition, drug release at medium containing 10% FBS was also studied, the result was shown in Figure S8, which was similar with the result in the medium without FBS as shown in Figure 4.

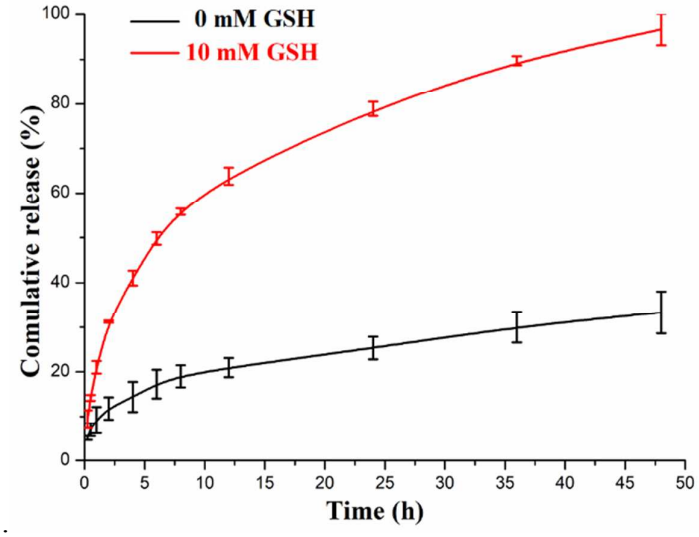

Figure 4. *In vitro* drug release of DOX-loaded polymeric micelles in medium contained 0 or 10 mM GSH

***In vitro* Cytotoxicity and Anticancer Activity**

The biocompatiability of polymeric micelle was performed with HeLa and 4T1 cells by MTT assay. As shown in Figure S9, both HeLa cells and 4T1 cells showed great cell viability even the concentration of polymeric micelles increased to 200 μg/mL, showing excellent biocompatiability of TPE-SS-PLAsp-*b*-PMPC copolymers, which could be attributed to the biomimetic zwitterionic PMPC shell of the micelles. Anticancer efficiency of free DOX and DOX-loaded micelles were investigated with various concentrations against HeLa and 4T1 cells for 24 h and 48 h. As shown in

Figure 5, DOX-loaded micelles showed lower inhibition efficiency than that of free DOX, which was due to the high initial inhibition efficiency of free DOX with full exposure to cells in 24 h. However, the tumor cells growth inhibition efficacy of drug-loaded micelles with more than 90% drug release after 48 h (Figure 4) was similar with that of free DOX, which indicated the great antitumor efficacy of DOX-loaded TPE-SS-PLAsp-*b*-PMPC micelles.

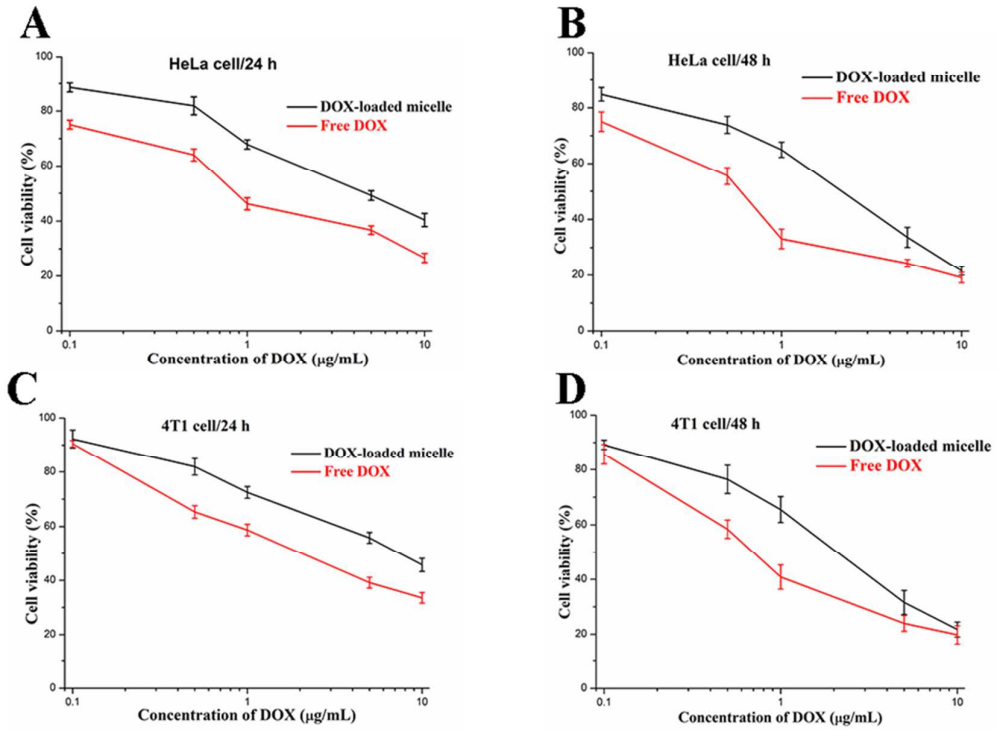

Figure 5. *In vitro* cytotoxicity of DOX-loaded micelles and free DOX against HeLa cells and 4T1 cells after incubation for 24 h and 48 h.

Cellular Imaging of TPE-SS-PLAsp-*b*-PMPC Micelles

The excellent biocompatibility of blank TPE-SS-PLAsp-*b*-PMPC micelles made it suitable for bioimaging. The AIE active cellular imaging of TPE-SS-PLAsp-*b*-PMPC micelles was investigated by CLSM. 4T1 cells were cultured with blank

TPE-SS-PLAsp-*b*-PMPC micelles with a final concentration of TPE at 40 μM for 2 h and 4 h and then observed by CLSM. Clear blue fluorescence could be seen due to the AIE character. As shown in Figure 6, the blue fluorescence of TPE groups was mainly located in the cytoplasm region of 4T1 cells, and the blue fluorescence intensity of TPE was significantly enhanced with the incubation time prelonged, suggesting the efficiently internalized of TPE-SS-PLAsp-*b*-PMPC micelles by cells. Additionally, CLSM imaging of HeLa cells was further performed to confirm the bioimaging ability of TPE-SS-PLAsp-*b*-PMPC micelles (Figure S10), which also exhibited great cellular imaging ability. Therefore, TPE-SS-PLAsp-*b*-PMPC micelles would be suitable for bioimaging.

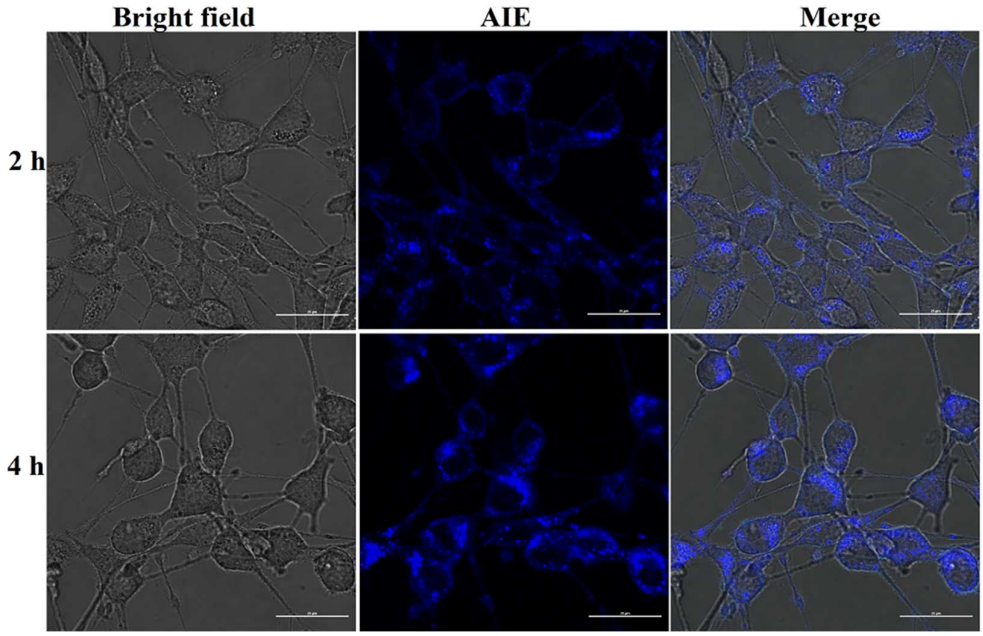

Figure 6. CLSM imaging of 4T1 cells after co-culture with TPE-SS-PLAsp-*b*-PMPC micelles for 2 and 4 h.

Cellular Uptake and Intracellular Drug Release

Efficient internalization was significant to drug carriers. The cellular uptake and

intracellular trace of DOX-loaded micelles were investigated by CLSM. As shown in Figure 7, both red fluorescent of DOX and blue fluorescent of TPE could be easily found in cytoplasm after incubation for 1 h, and the fluorescent became stronger with the incubation time increasing to 3 h and 5 h, which indicated that the cellular uptake of micelles was increased with time went on. Furthermore, obvious red fluorescence of DOX could be observed in the nuclei region after incubation for 7 h, which indicated the intracellular drug release from DOX-loaded micelles and subsequently delivered to the cell nuclei, suggesting the great AIE feature of TPE-SS-PLAsp-b-PMPC could be utilized to monitor the intracellular DOX delivery.

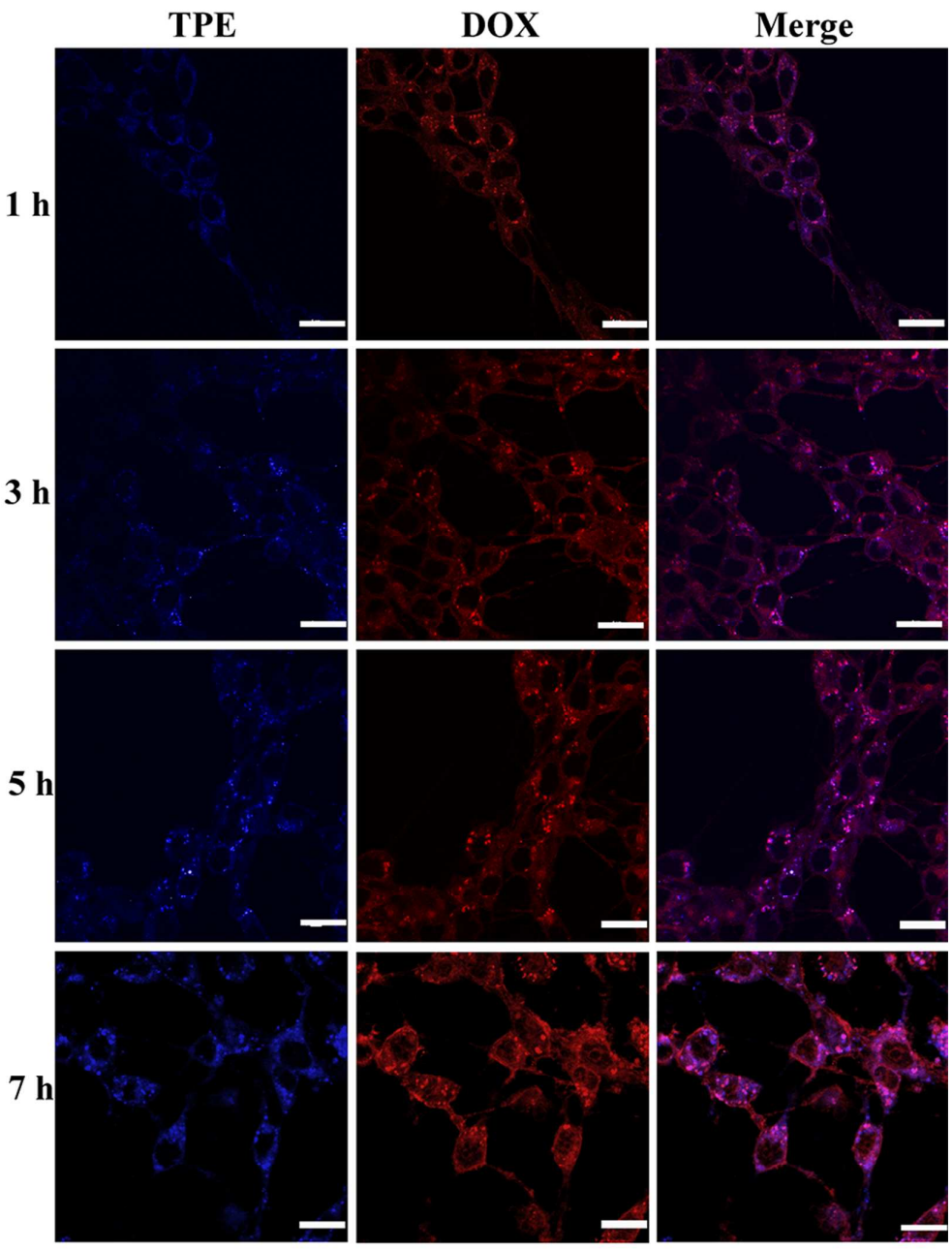

Figure 7. CLSM image of 4T1 cells cocultured with DOX-loaded TPE-SS-PLAsp-*b*-PMPC micelles for 1 h, 3 h, 5 h and 7 h. (scale bar 20 μm).

***In Vivo* Antitumor Activity**

BALB/c mice bearing 4T1 breast cancer tumors were used to evaluate the *in vivo* anti-tumor efficacy. Free DOX and DOX-loaded TPE-SS-PLAsp-*b*-PMPC micelles

were allowed to inject intravenously to mice with the dose of 5 mg DOX/kg body weight, and the same volume of saline solution was administered as the blank control. All the mice were alive before they were sacrificed and their body weights and tumor volumes were recorded continuously during the experimental period. The changes of tumor volumes were shown in Figure 8A, the tumor volumes of control group administered with saline solution increased rapidly, while both the free DOX treated and DOX-loaded TPE-SS-PLAsp-*b*-PMPC micelles treated groups exhibited effective inhibition in tumor growth compared to the control. More clearly, after 20 days, the average tumor volumes of control, free DOX and DOX-micelle groups were ~1700, 500 and 350 mm^3, respectively (*$p < 0.001$, **$p < 0.05$). In addition, the tumor volumes of DOX-loaded micelles group were smaller than that of free DOX, indicating the better antitumor efficacy of DOX-loaded TPE-SS-PLAsp-*b*-PMPC micelles than free DOX. Meanwhile, the body weight change of mice was used to reflect the DOX-related systemic toxicity. As shown in Figure 8B, a significant body loss was observed when the mice were treated with free DOX, showing serious systemic toxicity to the mice. While the body weight changes of mice did not show distinct difference in DOX-loaded micelles treatment group and the control group, indicating the limited side effects of DOX-loaded TPE-SS-PLAsp-*b*-PMPC micelles. After a treatment cycle, the tumors were harvested and the picture of tumors was showed in Figure 8C, which obviously confirmed the great antitumor efficacy of DOX-loaded micelles. The tumor inhibition rates were further calculated after the mice were sacrificed (Figure 8D), which further confirmed the better antitumor

efficacy of DOX-loaded micelles compared to free DOX. The great antitumor effect and lower drug-related toxicity confirmed the DOX-loaded micelle would be a good candidate for tumor therapy.

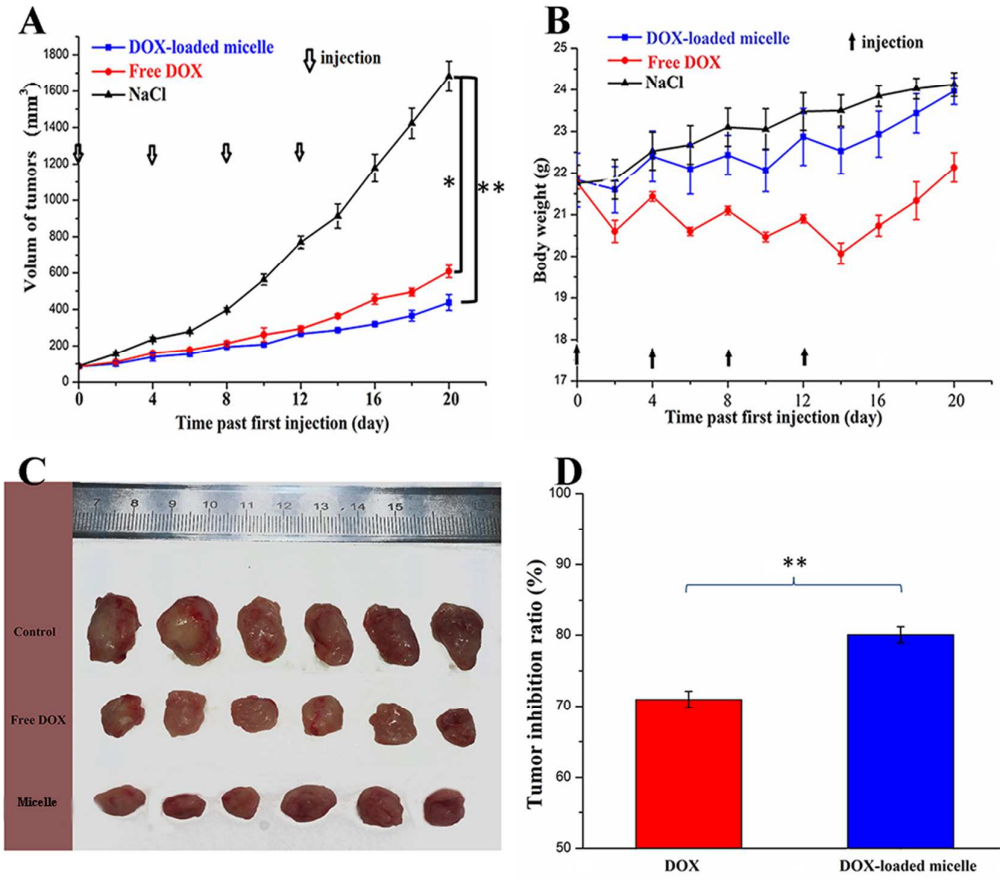

Figure 8. The *in vivo* antitumor activity of saline, free DOX and DOX-loaded TPE-SS-PLAsp-*b*-PMPC micelles. Volume changes of tumors after injection, data were presented as mean ± SD (n = 6). *P < 0.001; **P < 0.05 (A); Body weight changes of mice after injection (the arrows represented the injection time points) (B); Image of tumors after treatment for three weeks with different formulations (C); The inhibition rate of free DOX and DOX-loaded micelles treated groups compared with the control group (**p < 0.05) (D).

***EX Vivo* Optical Image Study**

To investigate the tumor-targeting ability of DOX-loaded TPE-SS-PLAsp-*b*-PMPC micelles in tumor-bearing mice, the *ex vivo* imaging of major organs (heart, liver, spleen, lung and kidney) and tumors treated by DOX-loaded micelles at different time intervals were performed by fluorescence imaging system (CRi, Inc.). As the result shown in Figure 9A, the major organs and tumor of control group did not show fluorescence, while the kidney, liver and tumor of mouse treated with DOX-loaded micelles showed strong fluorescence. Strong DOX fluorescence in tumor could be obvious observed at 12 h after intravenous injection of DOX-loaded micelles. Meanwhile, the signal of DOX was increased with time went on (Figure 9B), which was most evident at 48 h after treated with DOX-loaded micelles, indicating the long-circulating and continuous accumulation of micelles *in vivo* and effective remain of these DOX-loaded micelles. The fluorescence of DOX was also found in livers and kidneys, due to the metabolism. These results indicated that these DOX-loaded TPE-SS-PLAsp-*b*-PMPC micelles could rapid accumulate in tumor tissue via EPR effect and effective retention to inhibit tumor growth.

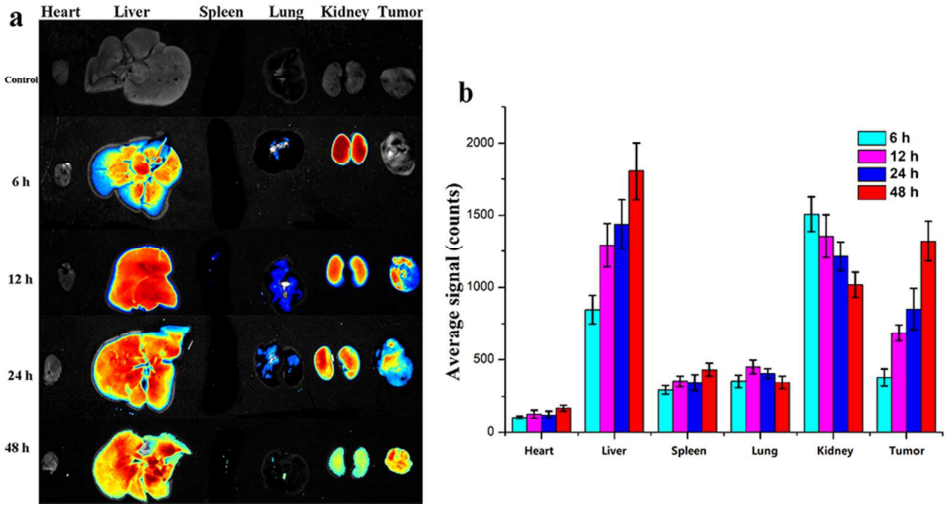

Figure 9. A) *EX vivo* imaging and biodistribution studies. DOX fluorescence images of tumor and organs at different time post injection of DOX-loaded micelle; B) Average signals collected from the major organs (heart, liver, spleen, lung and kidney) and tumors in tumor-bearing mice at different time points (n = 3).

Histological and Immunohistochemical Analyses

After 21 days, major organs and tumors from mice were collected and observed with hematoxylin and eosin (H&E) staining. As shown in Figure 10, similar with control group, no significant organs damages were found in DOX-loaded micelles treated mice. However, free DOX showed more obvious damage to major organs compared with control group and DOX-loaded micelles. Moreover, multifocal tumor metastases were observed in livers of mice treated with free DOX and saline. Mice treated with DOX-loaded micelles showed very few metastatic lesions. Therefore, these DOX-loaded TPE-SS-PLAsp-*b*-PMPC micelles would help to reduce the side effects of DOX and control tumor metastasis.

Immunohistochemical study was further used to evaluate the antitumor effects of DOX-loaded micelles and free DOX. CD31 was used to mark endothelial cells in blood vessels to reflect tumor angiogenesis and tumor microvessel density (MVD), which were closely associated with tumor growth, invasion and metastasis. As shown in Figure 11b, mice treated with DOX-loaded TPE-SS-PLAsp-*b*-PMPC micelles showed a significant lower MVD value than that of saline-treated mice and DOX-treated mice (*$p < 0.001$, **$p < 0.05$), indicating the DOX-loaded micelle would inhibit angiogenesis as well as inhibit tumor growth. The growth of tumor was

closely related to the proliferative cells in tumor. K_i-67 was a specific nuclear protein of proliferative cells, which was used to label the proliferative cells. As shown in Figure 10, mice treated with DOX-loaded micelles exhibited significant lower expression of *K*i-67 than control and free DOX treated mice (*$p < 0.001$, **$p < 0.05$), which was in accordance with *in vivo* antitumor studies. Therefore, DOX-loaded TPE-SS-PLAsp-*b*-PMPC micelles could limit the proliferation of tumor cells and improved antitumor efficacy.

TUNEL was used to confirm why tumor growth was inhibited in free DOX treated mice and DOX-loaded micelles treated mice. As shown in Figure 11, only small a number of apoptotic cells were observed in saline treated mice. However, DOX-loaded micelles had the highest ratio of apoptosis, with more than 70% of apoptotic cells was observed, indicating these DOX-loaded micelles would contribute to induce tumor apoptosis.

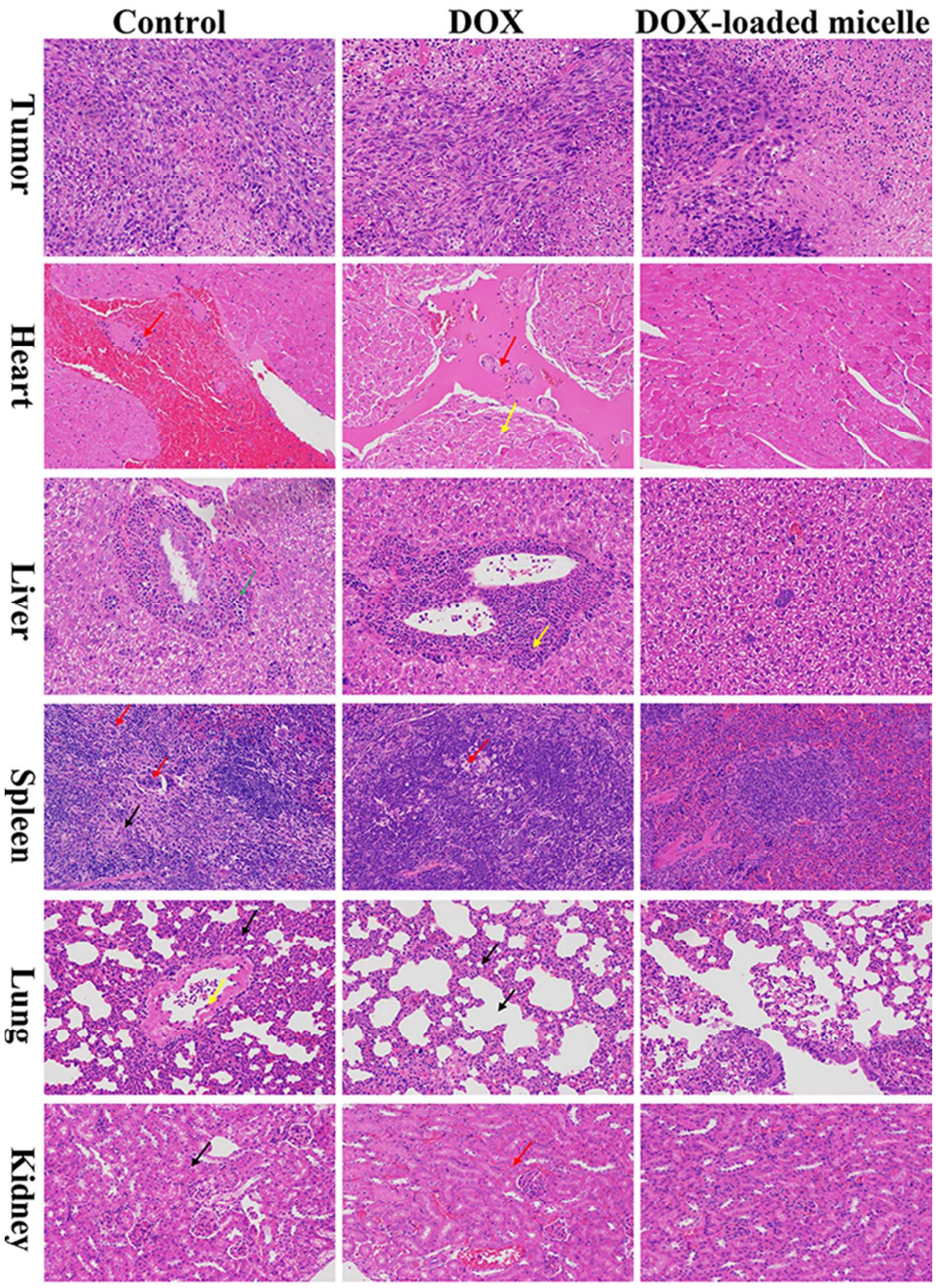

Figure 10. H&E staining assays for tumors, hearts, livers, spleens, lungs and kidneys after treatment with different administrations over 21 days (all tissues: 200×). The arrows indicated the damaged region of tissues.

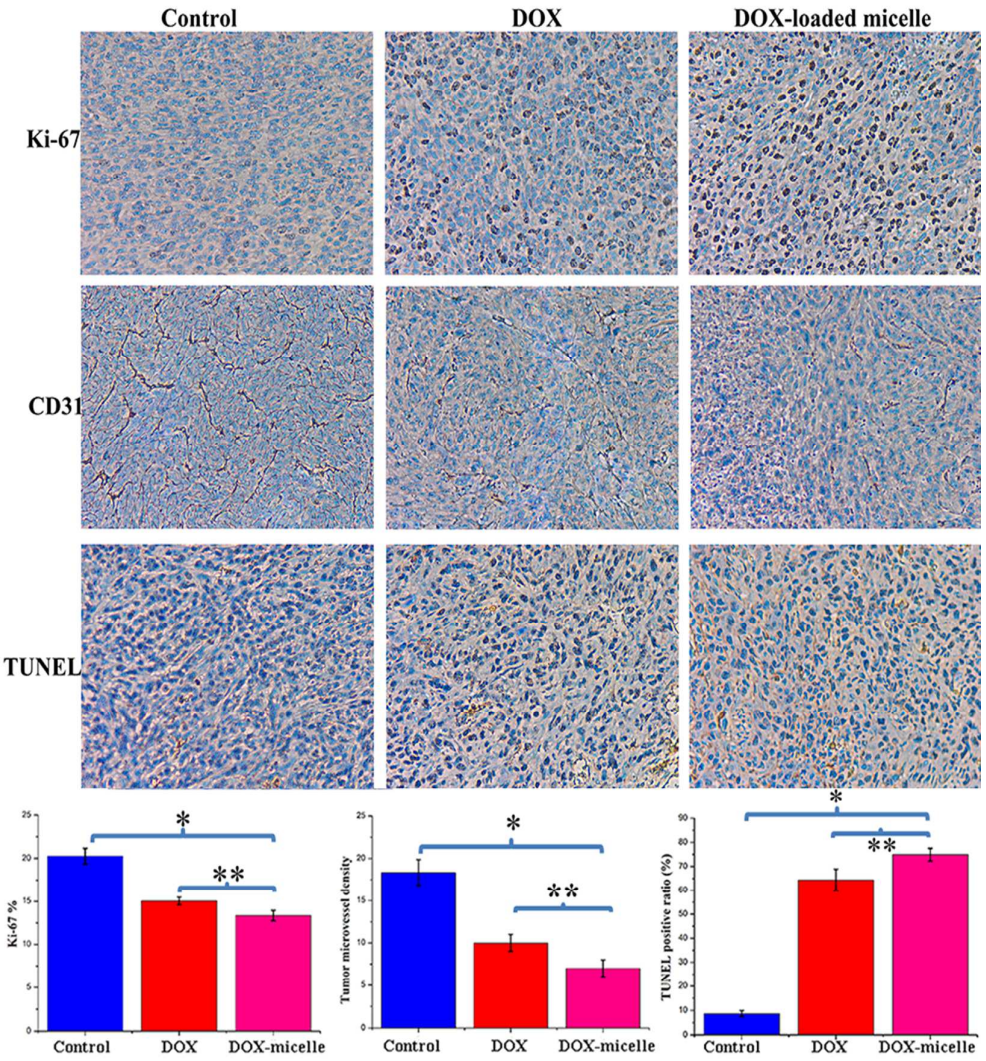

Figure 11. Histological and immunohistochemical analyses (*Ki*-67, CD31 and TUNEL) of tumor sections (× 400). The *Ki*-67 density in each image was calculated by *Ki*-67-positive area to total area, the CD31-positive area was expressed in endothelial cell pack and count capillary number by reading each section (MVD) and the apoptotic index was calculated as the ratio of the apoptotic cell number to the total tumor cell number in each field of view. Data were presented as mean ± SD (n = 6, *p < 0.001, **p < 0.05).

MATERIALS AND METHODS

MATERIALS

2-methacryloyloxyethyl phosphorylcholine (MPC) was purchased from Nanjing Natural Science and Technology Institute and used without further purification. Bis-(2-aminoethyl)disulfide dihydrochloride and Doxorubicin hydrochloride (DOX·HCl) were supplied by Sun Chemical Technology. (Shanghai, China) Co., Ltd. γ-benzyl-L-aspartate-N-carboxyanhydride (BLA-NCA) was synthesized as the reported literatures[39]. N-(2-aminoethyl)-2-bromo-2-methylpropanamide was acquired according to previous work[37]. N, N- Dimethylformamide (DMF) was refluxed with calcium hydride (CaH_2) for 3 h and purified by vacuum distillation. 3-(4, 5-Dimethyl-thiazol-2-yl)-2, 5-diphenyl tetrazolium bromide (MTT), cuprous bromide (CuBr), 2,2-Bipyridine (bpy) and other reagents were purchased from Best-Reagent (Chengdu, China) and used as received.

Synthesis of Poly (γ-Benzyl-L-Aspartate) Macroinitiator (PBLAsp-Br)

PBLAsp-Br was synthesized by ring-opening polymerization of BLA-NCA monomer with N-(2-aminoethyl)-2-bromo-2-methylpropanamide as initiator. Under an atmosphere of argon, BLA-NCA (5 g, 19 mmol) and initiator (0.2091 g, 1 mmol) were dissolved in 50 mL dry DMF in a dry flask. After stirring at room temperature for 3 days, the resulting solution was concentrated and poured into excess amount of cold diethyl ether. The precipitates were washed with diethyl ether for several times. The resultant PBLAsp-Br was dried under vacuum for 24 h.

Synthesis of Poly (γ-Benzyl-L-Aspartate)-block-Poly (2-Methacryloyloxyethyl

Phosphorylcholine) (PBLAsp-*b*-PMPC) Copolymer

The PBLAsp-b-PMPC copolymer was synthesised by ATRP of MPC with PBLAsp-Br as macroinitiator and CuBr/bpy as catalyst. Briefly, PBLAsp-Br initiator (0.9 g, 0.184 mmol), MPC (1.8 g, 6.102 mmol) and 20 mL of solvent (DMSO/MeOH, 1/1, v/v) were added to a dry flask. After four cycles of freeze-pump-thaw procedure, CuBr (26.5 mg, 0.184 mmol) and bpy (57.4 mg, 0.368 mmol) were added into the solution under the protection of argon and the reaction was allowed to perform at 40 ^{o}C for 2 days. The resultant crude product was purified by passing a neutral aluminum oxide column with the eluent of dimethyl formamide /methanol (1/2, v/v), concentrated, and precipitated into excess of cold ethyl ether. PBLAsp-*b*-PMPC was dried under vacuum for 24 h.

Preparation of Pure Pystamine

The pure cystamine was obtained by dehydrochloration of cystamine dihydrochloride according to literature[41]. Typically, cystamine dihydrochloride (4.5 g, 0.02 mol) was dissolved in 10 mL water in a 100 mL flask, then diethyl ether (Et_2O, 30 mL) and tetrahydrofuran (THF, 15 mL) were added. After cooling down in ice bath, 40% aqueous NaOH solution (40 g, 1 mol) was slowly added to the mixture solution. The oil layer was collected and the residue of aqueous layer was additionally extracted with a mixture of Et_2O (20 mL) and THF (10 mL). The combined organic phase was dried over NaOH and filtrated, the solution was removed by rotary evaporator to obtain pure cystamine.

Synthesis of Cystamine-conjugated Coly (Aspartate Acid)-block-Poly

(2-Methacryloyloxyethyl Phosphorylcholine) Copolymer (H_2N-SS-PLAsp-*b*-PMPC)

PBLAsp-*b*-PMPC (1 g, 0.08 mmol) was dissolved in 30 mL solution of DMSO/MeOH (1/1, v/v) at room temperature, and cystamine (1.3 g, 8 mmol) was added under the protection of argon. The solution was stirred for 36 h, concentrated by rotary evaporator and transferred into a dialysis bag (MWCO = 3500) and dialyzed against RO (pH ~ 5) water for 48 h. H_2N-SS-PLAsp-*b*-PMPC was obtained by lyophilizing.

Synthesis of TPE-conjugated TPE-SS-PLAsp-*b*-PMPC

4-nitrophenyl chloroformate-activated TPE (TPE-NO_2) was prepared according to previous work[40]. ^{13}C NMR (100 MHz, CD_3OD): 155.27, 150.86, 149.01, 145.59, 143.32, 143.23, 142.29, 141.83, 139.53, 132.55, 131.30, 131.23 127.83, 127.69, 126.69, 126.61, 125.39, 121.75, 119.85. High resolution ESI-MS: $[M + Na + H]^+$ calcd as 537.55, found 537.54.

PMPC-*b*-PLAsp-SS-NH_2 (0.4 g, 0.033 mmol) and TPE-NO_2 (0.4 g, 0.781 mmol) were dissolved in a mixture of DMF (12 mL) and MeOH (10 mL) at room temperature. 200 μL of TEA (1.446 mmol) were added under the protection of argon. The mixture was stirred for 36 h and subsequently allowed to concentrate by rotary evaporator, the resulting mixture was taken into a dialysis bag and dialyzed (MWCO = 3500) against RO water for 48 h and dried under vacuum to obtain the pure product.

Preparation of DOX-loaded Polymeric Micelles

The polymeric micelles were prepared by solvent exchange method. In brief,

TPE-conjugated copolymer (10 mg) and DOX (2 mg) (dehydrochlorinated as previous work[40]) were dissolved in a mixture of DMF/MeOH solvent (2 mL, v/v, 1/1). The mixture solution was added dropwise to 5 mL of RO water under strong stirring. After 30 min, the mixture was transferred into a dialysis bag (MWCO = 3500) and dialyzed against deionized water for 24 h at room temperature to remove the organic solvent and unloaded DOX. The solution was filtered through a 0.22 μm filter membrane and diluted to 1 mg/mL (copolymers). The drug loading efficiency (DLE) and drug loading content (DLC) were evaluated by previous method[35]. Blank polymeric micelles were prepared as the same way without the addition of DOX.

Redox-sensitive Behavior and *In Vitro* Drug Release

The redox-responsive behavior of TPE-SS-PLAsp-*b*-PMPC polymeric micelles was investigated with Dynamic Light Scattering (DLS) by monitoring the changes of particle sizes in the presence of GSH. Particularly, TPE-SS-PLAsp-*b*-PMPC micelles were incubated with 10 mM GSH at 37 ^{o}C, and the size changes of micelles were measured by DLS at preselected time intervals (0 h, 1 h, 2 h and 6 h). In addition, the influence of GSH on micellar structure was further investigated by TEM after incubation with 10 mM for 6 h. The *in vitro* release behavior of DOX was evaluated by dialysis method at 37 ^{o}C. In brief, 2 mL of DOX-loaded micelles (1 mg/mL) was transferred into a dialysis bag (MWCO = 3500) with 20 mL of PBS solution (pH 7.4) contained 0 or 10 mM GSH as release medium, respectively. The whole procedure of drug release was kept in the dark with constant shaking. At predetermined time interval, 2mL of release medium was taken out to measure the amount of released

DOX and the same amount of fresh medium was added subsequently. Additionally, drug release behavior was also studied in medium containing 10% FBS at pH 7.4.

In Vitro Cytotoxicity Studies

The *in vitro* cytotoxicity of blank TPE-SS-PLAsp-*b*-PMPC micelles and DOX-loaded micelles was evaluated by MTT assay against human cervical cancer (HeLa) cells and mouse breast cancer (4T1) cells. HeLa cells and 4T1 cells were seeded on 96-well plates at the density of 5000 per well with 200 μL of DMEM and RPMI-1640 medium, respectively. All the plates were incubated at 37 ^{o}C for 24 h in a balanced atmosphere with 5% CO_2. The same amount of fresh medium containing different concentrations of blank micelles, free DOX and DOX loaded micelles was allowed to replace the stale culture medium, and the cells were incubated for another 24 h or 48 h. The final concentration of blank micelles was ranged from 12.5 μg/mL to 200 μg/mL and the DOX concentration was ranged from 0.1 μg/mL to 10 μg/mL. The relative cell viability was detected by standard MTT assay and the absorbance of solutions was measured at 490 nm on a Bio-Rad microplate reader.

In Vitro Cellular Imaging

Confocal laser scanning microscopy (CLSM) was employed to study the cellular imaging of TPE-SS-PLAsp-*b*-PMPC micelles. 4T1 cells and HeLa cells cultured on a glass dish (diameter = 35 mm) (5×10^4 per dish) were allowed to incubated with micelles for 2 h and 4 h, and the final TPE concentration was 40 μM. Subsequently,

the cells were cleaned by PBS solution for 3 times followed by a small amount of PBS added. The cells were imaged by CLSM with excitation at 405 nm.

Cellular Uptake and Intracellular Drug Release

The cellular uptake of DOX-loaded micelles was studied by CLSM. 4T1 cells were planted on glass dishes (diameter = 35 mm) at a density of 2×10^4 per dish. After incubation for 24 h, DOX-loaded micelles were added with the final DOX concentration of 10 μg/mL. Cells were allowed to incubate for different predetermined time (1 h, 3 h, 5 h and 7 h) and washed with PBS for three times and a small amount of PBS supplemented. The cells were imaged by CLSM with excitation at λ = 405 nm and λ = 488 nm.

***Ex Vivo* Optical Image Study**

The xenograft tumor model was generated by subcutaneous injecting a suspension of 1×10^6 4T1 cells to each mouse. Free DOX or DOX-loaded TPE-SS-PLAsp-*b*-PMPC micelles (at doses of 5 mg DOX equivalent 1 kg of body weight) were intravenously administrated when the tumor volume reached about 300 mm^3, the mice were sacrificed and major organs (heart, liver, lung, spleen and kidney) and tumor were harvested by dissection after 6 h, 12 h, 24 h and 48 h injection. After washed with physiological saline for three times, the tumors and organs were performed with *in vivo* fluorescence imaging using a CRI Maestro Imaging System (Cambridge Research & Instrumentation, Inc., USA). All the processes of animal treatment were approved by the Sichuan Provincial Committee for Experimental Animal Management.

In Vivo Antitumor Effect

BALB/c mice (male, 18-20 g) were supplied by West China Experimental Animal Center of Sichuan University (China). Mice were treated with xenograft tumor by subcutaneous injecting a suspension of 1×10^6 4T1 cells in PBS buffer to the right back of mice. Mice were randomly grouped into 3 cages after the tumors approximately reached 100 mm^3 in volume. Mice were treated with NaCl saline solution, free DOX and DOX-loaded micelles (5 mg DOX equiv/kg) via the tail vein on days 0, 4, 8, and 12, respectively. The tumor size and body weight were simultaneously measured using a vernier caliper every two days, and the tumor volume was calculated using equation: $V = ab^2/2$, where a and b stood for the longest and shortest diameter of the tumors respectively. On the 21st day, all the mice were sacrificed and the major organs and tumors were collected, fixed in 4% neutral buffered formaldehyde for histological analysis[42]. Immunohistochemical studies were used to evaluate tumor inhibition via CD31, K_i-67 and TUNEL to reflect tumor angiogenesis, tumor cell proliferation and the apoptosis [43,44].

Measurements

The chemical structures were characterized by ^1H NMR spectra recorded on a spectrometer operating at 400 MHz (Bruker AMX-400). The particle size of the micelles was measured with a Malvern Zetasizer Nano ZS at room temperature. The molecular-weight distribution of PBLAsp-Br were determined by gel permeation chromatography (GPC) (HLC-8320) using DMF as the eluent at a flow rate of 1 mL/min at 40 ^oC and a series of narrow polymethyl methacrylate (PMMA) standards

for the calibration of the columns. Transmission electron microscopy (TEM) measurements were operated on a Hitachi H-600 transmission electron microscope with an accelerating voltage of 100 KV.

CONCLUSION

In this work, polymeric micelles for simultaneous bioimaging and intelligent drug delivery from TPE-conjugated redox-sensitive amphiphilic copolymer (TPE-SS-PLAsp-*b*-PMPC) have been developed. Antitumor drug DOX was encapsulated into the core of micelles during self-assemble process of this copolymer in aqueous medium. The uniform micelles of 87.3 nm with narrow distribution exhibited excellent stability in physiological conditions but sensitive to high level of GSH leading to trigger drug release. The TPE-conjugated TPE-SS-PLAsp-*b*-PMPC micelles showed great bioimaging ability and the intracellular drug delivery could be monitored. Moreover, through *ex vivo* imaging of major organs and tumors, we confirm these DOX-loaded micelles could efficiently accumulate in tumors and retain for a long time. Above all, these DOX-loaded micelles exhibited excellent antitumor efficacy and active imaging with much less side effects. Therefore, these AIE labeled redox response polymeric micelles provide a new alternative for simultaneous chemotherapy and bioimaging.

ACKNOWLEDGMENT

This research was financially supported by National Natural Science Foundation of

China (Projects 21502129), the National 111 Project of Introducing Talents of Discipline to Universities (No. B16033). We would be grateful to Chenghui Li (Analytical & Testing Center, Sichuan University) for help of taking laser scanning confocal images.

Supplementary Information

Figures showing ^{1}H NMR spectra, ^{13}C NMR spectra, GPC, UV-vis spectra, *in vitro* drug release, cytotoxicity and confocal laser scanning microscopy images.

REFERENCES

(1) Davis, M. E., Chen, Z. G., and Shin, D. M. (2008) Nanoparticle therapeutics: an emerging treatment modality for cancer. *Nat Rev. Drug. Discover 7*, 771-782.

(2) Choi, K. Y., Liu, G., Lee, S., and Chen, X. (2012) Theranostic nanoplatforms for simultaneous cancer imaging and therapy: current approaches and future perspectives. *Nanoscale 4*, 330-342.

(3) Blum, A. P., Kammeyer, J. K., Rush, A. M., Callmann, C. E., Hahn, M. E., and Gianneschi, N. C. (2015) Stimuli-responsive nanomaterials for biomedical applications. *J. Am. Chem. Soc. 137*, 2140-2154.

(4) Wei, H., Zhuo, R.-X., and Zhang, X.-Z. (2013) Design and development of polymeric micelles with cleavable links for intracellular drug delivery. *Prog. Polym. Sci.38*, 503-535.

(5) Maeda. H., Wu. J., Sawa, T., Matsumura, Y., Hori, K. (2000) Tumor vascular permeability and the EPR effect in macromolecular therapeutics: a review. *J.Control. Release 65*, 271-284.

(6) Maeda, H., Nakamura, H., and Fang, J. (2013) The EPR effect for macromolecular drug delivery to solid tumors: Improvement of tumor uptake, lowering of systemic toxicity, and distinct tumor imaging in vivo. *Adv. Drug. Deliver. Rev. 65*, 71-79.

(7) Kataoka, K., Harada, A., and Nagasaki, Y. (2012) Block copolymer micelles for drug delivery: Design, characterization and biological significance. *Adv. Drug. Deliver Rev. 64*, 37-48.

(8) Kim, T.-H., Jeong, G.-W., and Nah, J.-W. (2017) Preparation and anticancer effect of transferrin-modified pH-sensitive polymeric drug nanoparticle for

targeted cancer therapy. *J. Ind. Eng. Chem. 54*, 298-303.

(9) Cabral, H., and Kataoka, K. (2014) Progress of drug-loaded polymeric micelles into clinical studies. *J.Control. Release 190*, 465-476.

(10) Breul, A. M., Hager, M. D., and Schubert, U. S. (2013) Fluorescent monomers as building blocks for dye labeled polymers: synthesis and application in energy conversion, biolabeling and sensors. *Chem. Soc Rev. 42*, 5366-5407.

(11) Yuan, W. Z., Lu, P., Chen, S., Lam, J. W., Wang, Z., Liu, Y., Kwok, H. S., Ma, Y., and Tang, B. Z. (2010) Changing the behavior of chromophores from aggregation-caused quenching to aggregation-induced emission: development of highly efficient light emitters in the solid state. *Adv. Mater. 22*, 2159-2163.

(12) Hong, Y., Lam, J. W. Y., Tang,B. Z. (2011) Aggregation-induced emission. *Critical. Rev. 40*, 5361-5388.

(13) Zhang, X., Wang, K.; Chen, Y., and Wei, Y. (2015) Polymeric AIE-based nanoprobes for biomedical applications: recent advances and perspectives. *Nanoscale. 7*, 11486-11507.

(14) Shi, Y., Liu, M., Zhang, X., and Wei, Y. (2017) Recent progress and development on polymeric nanomaterials for photothermal therapy: a brief overview. *J. Mater. Chem B*. 5, 194-206.

(15) Cho, H., Bae, J., Garripelli, V. K., Anderson, J. M., Jun, H. W., and Jo, S. (2012) Redox-sensitive polymeric nanoparticles for drug delivery. *Chem. Commun. 48*, 6043-6045.

(16) Kozlovskaya, V., Liu, F., Xue, B., Ahmad, F., Alford, A., Saeed, M., and Kharlampieva, E. (2017) Polyphenolic polymersomes of temperature-sensitive poly(N-vinylcaprolactam)-block-poly(N-vinylpyrrolidone) for anticancer therapy. *Biomacromolecules 18*, 2552-2563.

(17) Felber, A. E., Dufresne, M. H., and Leroux, J. C. (2012) pH-sensitive vesicles, polymeric micelles, and nanospheres prepared with polycarboxylates. *Adv. Drug. Deliver Rev. 64*, 979-992.

(18) Rica, R. de la., Aili, D., Stevens, M. M. (2012) Enzyme-responsive nanoparticles for drug release and diagnostics. *Adv. Drug. Deliver. Rev 64*, 967-978.

(19) Meng, F.; Zhong, Z.; Jan, F. (2009) Stimuli-responsive polymersomes for programmed drug delivery. *Biomacromolecules***.** 10, 198-209.

(20) Li, J., Huo, M., Wang, J., Zhou, J., Mohammad, J. M., Zhang, Y., Zhu, Q., Waddad, A. Y., Zhang, Q. (2012) Redox-sensitive micelles self-assembled from amphiphilic hyaluronic acid-deoxycholic acid conjugates for targeted intracellular delivery of paclitaxel. *Biomaterials***.** *33*, 2310-2320.

(21) Chen, Q.; Zheng, J.; Yuan, X.; Wang, J.; Zhang, L. (2018) Folic acid grafted and tertiary amino based pH-responsive pentablock polymeric micelles for targeting anticancer drug delivery. *Mater. Sci Eng C*. 82, 1-9.

(22) Shi, C.; Guo, X.; Qu, Q.; Tang, Z.; Wang, Y.; Zhou, S. (2014) Actively targeted delivery of anticancer drug to tumor cells by redox-responsive star-shaped micelles. *Biomaterials***.** *35*, 8711-8722.

(23) Cheng, R.; Meng, F.; Deng, C.; Klok, H. A.; Zhong, Z. (2013) Dual and

multi-stimuli responsive polymeric nanoparticles for programmed site-specific drug delivery. *Biomaterials. 34*, 3647-3657.

(24) Chen, J.; Zehtabi, F.; Ouyang, J.; Kong, J.; Zhong, W.; Xing, M. M. Q. (2012) Reducible self-assembled micelles for enhanced intracellular delivery of doxorubicin. *J. Mater. Chem. 22* , 7121-7129.

(25) Meng, F.; Hennink, W. E.; Zhong, Z. (2009) Reduction-sensitive polymers and bioconjugates for biomedical applications. *Biomaterials. 30*, 2180-2198.

(26) Zhang, X.; Liu, K.; Huang, Y.; Xu, J.; Li, J.; Ma, X.; Li, S. (2014) Reduction-sensitive dual functional nanomicelles for improved delivery of paclitaxel. *Bioconjugate Chem. 25*, 1689-1696.

(27) Hoffman, A. S. (2008) The origins and evolution of "controlled" drug delivery systems. *J.control Release. 132*, 153-163.

(28) Xiao, K.; Li, Y.; Luo, J.; Lee, J. S.; Xiao, W.; Gonik, A. M.; Agarwal, R. G.; Lam, K. S. (2011) The effect of surface charge on in vivo biodistribution of PEG-oligocholic acid based micellar nanoparticles. *Biomaterials. 32*, 3435-3446.

(29) Bae, Y.; Kataoka, K. (2009) Intelligent polymeric micelles from functional poly(ethylene glycol)-poly(amino acid) block copolymers. *Adv Drug Deliver Rev. 61*, 768-784.

(30) Hrkach, J., Holf, D. V., Ali, M. M. (2012) Preclinical development and clinical translation of a PSMA-targeted docetaxel nanoparticle with a differentiated pharmacological profile. *Nanomedicine*. *4* , 128ra39.

(31) Harris, J. M.; Chess, R. B. (2003) Effect of pegylation on pharmaceuticals. *Nat. Rev. 2*, 214-221.

(32) Knop, K.; Hoogenboom, R.; Fischer, D.; Schubert, U. S. (2010) Anwendung von Poly(ethylenglycol) beim Wirkstoff-Transport: Vorteile, Nachteile und Alternativen. *Angew. Chem*. *122*, 6430-6452.

(33) Jin, Q.; Chen, Y.; Wang, Y.; Ji, J. (2014) Zwitterionic drug nanocarriers: a biomimetic strategy for drug delivery. *Colloid Surface. B. 124*, 80-86.

(34) Chen, S.; Zheng, J., Li, L and Jiang, S. (2005) Strong resistance of phosphorylcholine self-assembled monolayers to protein adsorption: insights into nonfouling properties of zwitterionic materials. *J. Am. Chem. Soc*. *127*, 14473-14478.

(35) Huang, Z.; Cang, H.; Huang, R.; Cai, Z.; Zhang, H. (2014) Amphiphilic block copolymer poly(2-methacryloyloxyethyl phosphorylcholine) and poly(trimethylene carbonate): Preparation and for intracellular drug delivery. *Polym.Sci.Ser B*. *56*, 883-894.

(36) Wang, H.; Liu, G.; Gao, H and Wang, Y. (2015) A pH-responsive drug delivery system with an aggregation-induced emission feature for cell imaging and intracellular drug delivery. *Polym. Chem*. 6, 4715-4718.

(37) Liu, G.; Zhuang, W.; Chen, X.; Yin, A.; Nie, Y.; Wang, Y. (2016) Drug carrier system self-assembled from biomimetic polyphosphorycholine and biodegradable polypeptide based diblock copolymers. *Polymer. 100*, 45-55.

(38) Zhao, Y.; He, G.; Guo, W.; Bao, L.; Yi, M.; Gong, Y.; Zhang, S. (2016)

Self-assembled micelles prepared from amphiphilic copolymers bearing cell outer membrane phosphorylcholine zwitterions for a potential anti-phagocytic clearance carrier. *Polym. Chem. 7*, 5698-5708.

(39) Daly, W. H., Poche',D.; Rouge, B. (1988) The preparation of N-carboxyanhydrides of α-amino acids using bis(trichloromethyl)carbonate. *Tetrahedron Let. 29*, 5859-5862.

(40) Zhuang, W.; M, B.; Liu, G.; Li, G.; Wang, Y. (2017) TPE-conjugated biomimetic and biodegradable polymeric micelle for AIE active cell imaging and cancer therapy. *J. Appl Polym Sci. 45651*.

(41) Alferiev, I. S.; Connolly, J. M.; Levy, R. J. (2005) A novel mercapto-bisphosphonate as an efficient anticalcification agent for bioprosthetic tissues. *J. Organometa Chem. 690*, 2543-2547.

(42) Rumayor, A.; Carlos, R. (2015) Ghost cells in pilomatrixoma, craniopharyngioma, and calcifying cystic odontogenic tumor: histological, immunohistochemical, and ultrastructural study. *J. Oral. Pathol Med.* 44, 284-290.

(43) Tinnikov, A. A.; Yeung, K. T.; Das, S.; Samuels, H. H. (2009) Identification of a novel pathway that selectively modulates apoptosis of breast cancer cells. *Cancer Res.* 69, 1375-1382.

(44) Urruticoechea, A.; Smith, IE.; Dowsett, M. (2009) Proliferation marker Ki-67 in early breast cancer. *J. Modern Oncol*. 23, 7212-7220.

(45) Hu, R., Erik, Lager., Eduardo, Pen˜a-Cabrera and Tang, B. Z. (2009) Twisted intramolecular charge transfer and Aggregation-Induced Emission of BODIPY derivatives. *J. Phys. Chem. C.* 113, 15845–15853.

(46) Xue, X., Zhao, Y., Zou, G., and Liang, X. (2014) Spatiotemporal drug release visualized through a drug delivery system with tunable Aggregation-Induced Emission. *Adv Mater*. 26 (5).

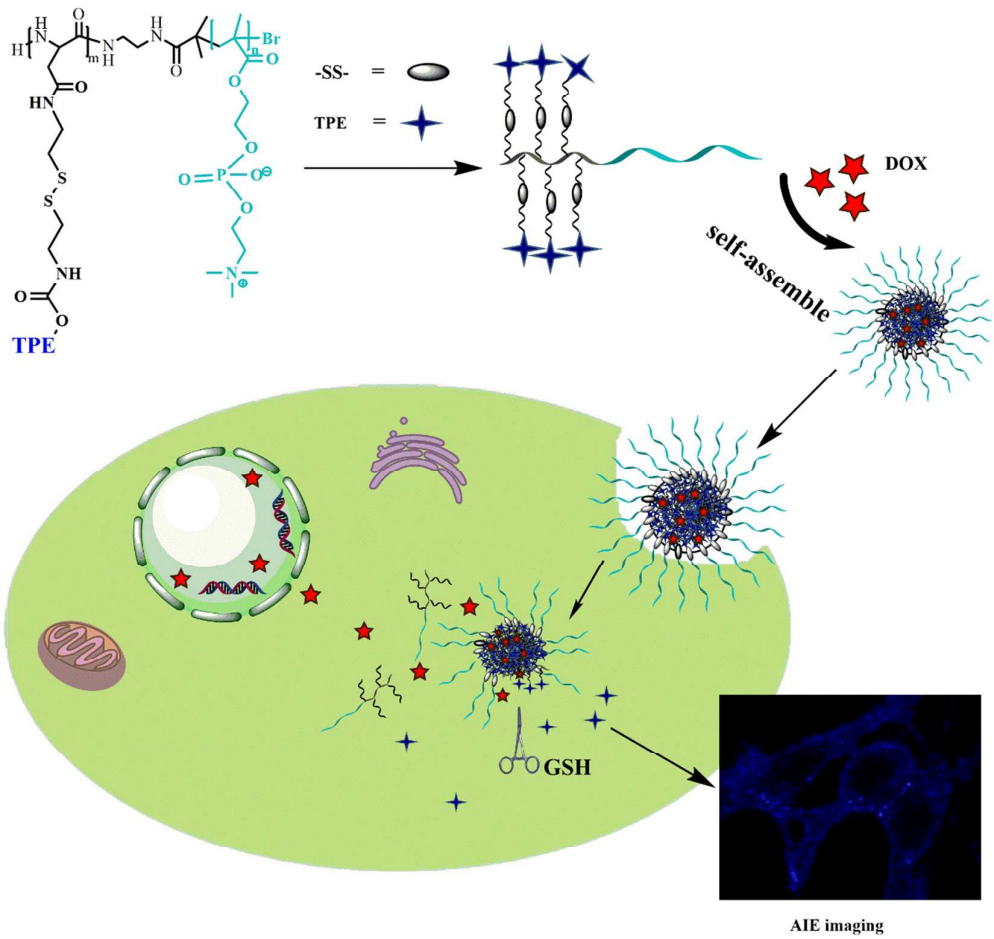

The redox-responsive biomimetic polymeric micelle (TPE-SS-PLAsp-*b*-PMPC) with AIE active imaging was introduced to develop an anticancer drug delivery as well as diagnosis therapy. For its unique AIE nature and quick response to the high concentration of GSH, the DOX-loaded TPE-SS-PLAsp-*b*-PMPC micelles exhibited great environment triggered drug release and cellular imaging, which make

TPE-SS-PLAsp-*b*-PMPC micelle a good candidate for simultaneous anticancer treatment and diagnosis.